

1 A continuous stable isotope record from the Penultimate glacial maximum
2 to the Last Interglacial (159 to 121 ka) from Tana Che Urla Cave (Apuan
3 Alps, central Italy)

4
5 Eleonora Regattieri^{*,1,2}, Giovanni Zanchetta^{1,2,3}, Russell N. Drysdale⁴, Ilaria Isola³,
6 John C. Hellstrom⁵, Adriano Roncioni⁶

7 *Corresponding author, regattieri@dst.unipi.it , 0039 050 2215795

8 ¹Dipartimento di Scienze della Terra, Via S. Maria 53 56126 Pisa, Italy

9 ²Istituto di Geoscienze e Georisorse IGG-CNR, via Moruzzi 1, 56100 Pisa, Italy

10 ³Istituto Nazionale di Geofisica e Vulcanologia INGV, Via della Faggiola 32, Pisa Italy

11 ⁴Department of Resource Management and Geography, University of Melbourne, Victoria 3010,
12 Australia

13 ⁵School of Earth Sciences, University of Melbourne, Victoria 3010 Australia

14 ⁶Gruppo Speleologico Lucchese, via Don Minzoni, Lucca

15

16

17

18

19

20

21

22

23

24 **Abstract**

25 Relatively few radiometrically dated records are available for the central Mediterranean spanning
26 the marine isotope stage 6-5 (MIS 6-5) transition and the first part of the Last Interglacial. Two
27 flowstone cores from Tana che Urla Cave (TCU, central Italy), constrained by 19 U/Th ages,
28 preserve an interval of continuous speleothem deposition between ca. 159 and 121 ka. A multiproxy
29 record ($\delta^{18}\text{O}$, $\delta^{13}\text{C}$, growth rate and petrographic changes) obtained from this flowstone preserves
30 significant regional-scale hydrological changes through the glacial/interglacial transition and multi-
31 centennial variability (interpreted as alternations between wetter and drier periods) within both
32 glacial and interglacial stages. The glacial stage shows a wetter period between ca. 154 and 152 ka,
33 while the early to middle Last Interglacial period shows several drying events at ca. 129, 126 and
34 122 ka, which can be placed in the wider context of climatic instability emerging from North
35 Atlantic marine and NW European terrestrial records. The TCU record also provides important
36 insights into the evolution of local environmental conditions (i.e. soil development) in response to
37 regional and global-scale climate events.

38
39 Key words: Speleothem, Stable isotopes, Central Italy, penultimate deglaciation, Last Interglacial

40
41 **Introduction**

42 The timing and climatic evolution of the penultimate deglaciation (Termination II in the deep-sea
43 sediment record) and the succeeding interglacial (MIS 5e) are relevant to understanding both the
44 mechanisms of ice-age cycles in general and, more specifically, the background of natural climate
45 variability during interglacials and how the present interglacial may come to an end (e.g. Kukla et
46 al., 1997, 2002; Broecker and Henderson, 1998; Tzedakis 2009). In particular, there is increasing
47 evidence that the climate of the Last Interglacial was unstable relative to the Holocene. This
48 variability was first identified in North Atlantic marine sediments (e.g. McManus et al., 1994; Oppo
49 et al., 2001; Heusser and Oppo, 2003; Bond et al. 2001) and, at least for the most prominent events,

50 this instability propagated into southern Europe and the Mediterranean basin (e.g. Martrat et al.,
51 2004; Sanchez-Goñi et al., 2005; Sprovieri et al., 2006; Brauer et al., 2007; Couchoud et al., 2009).
52 This instability has been related to hydrographic changes in the dynamics of the North Atlantic
53 Meridional Overturning Circulation (MOC). However, the timing and geographical persistence of
54 MIS 5e variability is still relatively poorly known, with many of the climatic oscillations yet to be
55 identified and their impacts still poorly understood beyond the North Atlantic region. In particular,
56 independently (e.g. radiometrically) dated records of the penultimate deglaciation and Last
57 Interglacial in the Mediterranean basin are rare (e.g Bar-Matthews et al. 2000; Drysdale et al., 2005,
58 2009; Vogel et al., 2009; Lezine et al., 2010) and, in this context, the most chronologically robust
59 archives for paleoclimate reconstruction on land have been speleothems, because of their well-
60 demonstrated high sensitivity to climate changes and their capability to be dated precisely by U/Th
61 methods (e.g. Richards and Dorale, 2003; Bar-Matthews et al., 1999).

62 In this study we present petrographic, growth rate and stable isotope data from two flowstone cores
63 collected from Tana che Urla Cave (TCU, Apuan Alps NW Tuscany, central Italy, Fig. 1), which
64 show continuous growth between ca. 159 and 121 ka. The aim of this work is to investigate the
65 regional hydrological changes occurring at the glacial/interglacial transition and to investigate the
66 presence of centennial-scale variability during both the penultimate glacial and the first part of the
67 Last Interglacial.

68

69 **Cave Setting**

70 Tana che Urla (TCU) (Fig. 1) is a sub-horizontal spring cave (592 m of total length, of which 370 m
71 is emerged and 222 m is submerged; 45 m of total height difference) that opens at 620 m a.s.l. on
72 the south-eastern side of the Pania massif, in the Apuan Alps (NW Tuscany, central Italy). The cave
73 has developed at the contact between metasiliclastics and schists (Fornovolasco schist formation),
74 and Triassic meta-dolomite (known as the Grezzoni formation, Pandeli et al., 2004). Inside the cave

75 there is a permanent stream, which represents the terminal part of an underground collector system
76 that drains the southern slope of Pania della Croce Mountain (1858 m a.s.l.).
77 The valley above the cave is covered by forest, mainly of cultivated chestnuts (*Castanea sativa*) at
78 lower altitude, and beech (*Fagus sylvatica*) at higher altitude; the summit part (above ca. 1600 m
79 a.s.l.) hosts a grassland dominated by the genus *Brachipodium*. All plants belong to the C3-type
80 vegetation category.

81 The local climate is wet throughout the year, with a mean annual precipitation of about 2500 mm/yr
82 recorded at the nearby village of Fornovolasco (data spanning 1951 to 1995: Piccini et al., 1999) but
83 higher (more than 3000 mm/yr) on the ridge of Pania della Croce. Such high precipitation is due to
84 the strong Apuan Alps orographic effect, which traps eastward-moving moisture. Analyses of air-
85 mass back trajectories show that the western Mediterranean and North Atlantic are the dominant
86 sources of local rainfall (Drysdale et al., 2004). There is no official temperature record nearby, but
87 the mean annual temperature (MAT) of the site recorded inside the cave (discontinuously monitored
88 since 2008; n=7) is 10.2°C (SD 0.5°C).

89 Irregular samples of drip waters collected in recent years show a near-constant oxygen isotope
90 composition ($-7.13 \pm 0.27\text{‰}$, n=7). Based on previous work by Mussi et al. (1998), these values are
91 consistent with a local recharge area at ca. 800-700 m a.s.l. and a rain-shadow effect on the isotopic
92 composition of meteoric precipitation exerted by Apennine divide.

93

94 **Materials and Methods**

95 Two cores, TCU-D3 and TCU-D4 (Fig. 2, herein referred to as D3 and D4), were drilled about 1.5
96 m from one another, from the same flowstone mass located in the main branch of the cave. Core D3
97 was drilled from a lower angle, lower lobe of the flowstone, whereas the lobe from which D4 was
98 extracted is located in a steeper part of the flowstone. The sample location is ca. 100 m from the
99 cave entrance, on the left bank of the cave stream, ca. 3 m above the current river level. D4 and D3
100 are 350 mm and 640 mm long respectively. In both cores the bedrock was reached.

101 Polished sections of each core were sub-sampled for stable C and O isotope ($\delta^{18}\text{O}$ and $\delta^{13}\text{C}$)
102 analyses perpendicular to the growth laminations. D4 was sampled at 1 mm increments using a
103 milling machine with a 1 mm-diameter drilling bit, producing 350 samples. D3 was sampled with a
104 manual drill (1 mm-diameter drilling bit) at ca. 1.5 to 2.0 mm increments, producing 393 samples.
105 $\delta^{18}\text{O}$ and $\delta^{13}\text{C}$ isotope ratios were measured using a GV2003 continuous-flow isotope ratio mass
106 spectrometer at the University of Newcastle, Australia. All results are reported relative to the
107 Vienna Pee Dee Belemnite (V-PDB) international scale. Sample results were normalised to this
108 scale using a Carrara Marble standard (NEW1) previously calibrated using the international
109 standards NBS-18 and NBS-19. Analytical uncertainty for $\delta^{18}\text{O}$ and $\delta^{13}\text{C}$ were 0.09 ‰ and 0.05‰
110 respectively.

111 Nineteen samples from both cores were taken for U/Th dating. Owing to the likelihood of large
112 uncertainties in the results due to clastic contamination and low uranium content in the flowstone,
113 solid prisms of ca. 200 mg (ca. 3 mm wide along the lamina and 1 mm thick on growth axis) were
114 used. The U/Th dating was performed at the University of Melbourne (Victoria, Australia)
115 following the method of Hellstrom (2003). Briefly, samples were dissolved and a mixed ^{236}U - ^{233}U -
116 ^{229}Th spike was added prior to removal of the carbonate matrix with ion-exchange resin. The
117 purified U and Th fraction was introduced in a dilute nitric acid to a multi-collector inductively
118 coupled plasma–mass spectrometer (MC-ICPMS, Nu-Instruments Plasma). The $^{230}\text{Th}/^{238}\text{U}$ and
119 $^{234}\text{U}/^{238}\text{U}$ activity ratios were calculated from the measured atomic ratios using an internally
120 standardised parallel ion-counter procedure and calibrated against the HU-1 secular equilibrium
121 standard. Correction for detrital Th content was applied using initial activity ratios of detrital
122 thorium ($^{230}\text{Th}/^{232}\text{Th}$)_i of 2.55 ± 0.80 and 2.95 ± 0.45 for D4 and D3 respectively. These values and
123 their relative 2σ uncertainty were calculated using a Monte Carlo ‘stratigraphic constraint’
124 procedure based on the series of U/Th ages from both cores (Hellstrom 2006). Under this method,
125 the ($^{230}\text{Th}/^{232}\text{Th}$)_i and its uncertainty are optimized in order to bring all ages into correct
126 stratigraphic order (i.e. with the assumption that age must increase with depth from top) within their

127 age uncertainties. A depth-age model (Fig. 3) for core D4 was constructed using a Bayesian Monte
128 Carlo approach (Drysdale et al. 2005; Scholz et al. 2012).

129

130 **Results**

131 The chronology of D4 is better constrained compared to D3, which seems to be more affected by
132 clastic contamination (Table 1), perhaps because the flowstone lobe from where D3 was taken is
133 inclined at a lower angle than D4 site, facilitating a greater build up and incorporation of detrital
134 particles during calcite deposition. Consequently, after preliminary dating, the process of improving
135 the age model was achieved by a greater focus on core D4. Age constraints indicate that D4 shows
136 continuous growth between ca. 158.5 ± 2.7 and 121.4 ± 3.0 ka and henceforth will be considered as
137 the 'master core'. Herein, we focus mostly on the basal section (237 mm) of D4. The upper section
138 of both cores display several growth interruptions and their age profiles are poorly constrained,
139 warranting only brief discussion.

140

141 *Stratigraphy*

142 Both cores (Fig. 2) are mainly composed of columnar calcite, which ranges from poorly-to-well
143 laminated to massive, often with a persistent detrital component. Based on the clastic content,
144 fabrics, visual appearance and color of the calcite, Regattieri et al. (2012) defined two main
145 lithofacies (Fig. 4). Lithofacies (Lf) A is richest in clastic material and is characterised by grey-
146 brown calcite with thin laminations of sediment, while Lf-B is composed of compact, milky calcite,
147 with little to no evidence of lamination and a lower content of impurities. Following Regattieri et al.
148 (2012), the discussed sections of D4 and D3 show a basal portion of Lf-A that spans from the start
149 of the deposition at ca. 159 ka to ca. 132 ka (depth 348-208 mm on D4 and 639-439 mm on D3,
150 ages from the D4 age model), followed by Lf-B until the first growth interruption (Hiatus Hs1) at
151 ca. 121 ka (depth 95 mm on D4, 299 mm on D3). This hiatus is clearly recognizable in both cores
152 (Hs1 in Figs 2, 4) and marks the end of the interval discussed here. The upper part of both cores

153 shows further alternation between the two defined lithofacies, although the sequence is thicker in
154 core D3, and also contains another type of calcite that is more porous and contains microgour
155 remnants (Lf-C of Regattieri et al., 2012).

156

157 *Chronology*

158 TCU speleothems are characterized by a low uranium content (average concentration in both cores
159 is 42 ppb, minimum = 18 ppb, maximum = 89 ppb; see Table 1) and persistent detrital
160 contamination (i.e. low $^{230}\text{Th}/^{232}\text{Th}$, see Table 1), which is particularly pronounced in the Lf-A
161 lithofacies (Regattieri et al., 2012). The 13 corrected ^{230}Th ages of the lower section of core D4
162 range from 159.1 ± 1.3 ka before present to 120.4 ± 5.4 ka (Fig. 2 and Table 1). Six ages from the
163 upper section of D4, above the Hs1 hiatus, indicates brief intervals of late MIS 5, Late Glacial and
164 Holocene growth (Fig. 2).

165 Four of the six corrected ^{230}Th ages on core D3 range from 144.1 ± 4.0 ka to 100.3 ± 3.0 ka, and are
166 in stratigraphic order. Three of these are contained in the lower section (before hiatus Hs1, see Fig.
167 2 and Table 1) and one just above the hiatus. Two further ages from this core (Table 1 and Fig. 2)
168 are reported only for completeness but, due to their large errors, they do not add useful information
169 to this study. Hiatus Hs1, which marks the end of the discussed interval, is constrained in core D4 to
170 between ca. 121.4 ± 2.0 and 112.5 ± 2.8 ka.

171 The upper section of the TCU flowstone shows discontinuous growth for late MIS 5, with
172 deposition at ca. 112.5 ± 2.8 ka in core D4 and at 100.3 ± 3.0 ka in core D3. Stratigraphic correlation
173 between the two cores (Regattieri et al., 2012) suggests that these two ages should represent the
174 same interval of continuous growth. Core D4 grows continuously also between ca. 81.1 ± 2.6 ka and
175 75.0 ± 0.8 ka. Growth in the terminal part of the two cores is disturbed by a series of interruptions,
176 none of which are fully chronologically constrained but with clear evidence in thin section of
177 erosion and mud deposition (Regattieri et al., 2012). Two ages indicate discontinuous growth at ca.
178 12.6 ± 0.7 ka and 7.8 ± 0.3 ka.

179 The growth rate in D4 (Fig. 5) shows initial values of ca. 8.8 mm/ka followed by a peak of 10.5
180 mm/ka at ca. 153.5±1.9 ka. This peak is succeeded by a very low growth rate (average ca. 3.3
181 mm/ka) until ca. 130 ka, after which it increases dramatically to up to ca. 20 mm/kyr (between ca.
182 130 and 127 ka). After ca. 127 ka, the growth rate decreases abruptly in two subsequent steps: until
183 ca. 9 mm between ca. 126-125 ka and then to 3-3.5 mm/ka from ca. 124 ka to the Hs1.

184

185 *Stable isotopes*

186 The $\delta^{13}\text{C}$ and $\delta^{18}\text{O}$ variations measured in D4 and D3 vs. depth from top (mm) are shown in Fig. 4,
187 whilst the stable isotope composition vs. age for the discussed section of D4 is displayed in Fig. 5.
188 The $\delta^{18}\text{O}$ values range from -2.79‰ to -6.28‰ in D4 and from -2.47‰ to -6.32‰ in D3, whilst the
189 $\delta^{13}\text{C}$ values range from -2.24‰ to -10.74‰ in D4 and from -1.04‰ to -10.69‰ in D3. Isotope
190 profiles from the lower section of both cores show substantially the same pattern of variations,
191 although sometimes with different degrees of compression (vs. distance) for the same oscillations.
192 The record starts with $\delta^{18}\text{O}$ values of ca. -3.8 ‰ and there is a peak of lower values (average ca. -
193 4.5‰) which starts at ca. 154.0±2.0 ka and terminates abruptly around ca. 151.6±2.2 ka. Thereafter
194 follows an interval of generally higher values between ca. 151.4±1.9 and ca. 132.2 ±1.2 ka, with
195 consistent millennial variability ($\delta^{18}\text{O}$ difference of average 0.7‰) and a slight trend towards lower
196 values from ca. 139.9 ±2.7 ka. The most prominent feature of the oxygen record, however, starts at
197 ca. 132.1±1.8 ka, when a dramatic excursion of ca. 3 ‰ towards lower values occurs, which peaks
198 at ca. 131.0 ±1.2 ka. A narrow and sharp positive peak centered at ca. 129.6±1.0 ka is followed by
199 the interval of lowest values, which lasts between ca. 129.4±1.0 and 126.7±1.2 ka. At ca. 126.1±1.3
200 ka there is another excursion to higher values (ca. 0.7 ‰) lasting ca. 0.9 ka, and then an interval of
201 lower values which persist until ca. 123.6±1.2 ka. After this interval in both cores the $\delta^{18}\text{O}$ values
202 increase sharply (ca. 1.2 ‰) and then remain stable until hiatus Hs1 (ca. 121.4 ±2.0 ka) which
203 marks the end of the discussed interval.

204 The $\delta^{13}\text{C}$ record closely follows the major changes in $\delta^{18}\text{O}$, that is, all of the prominent features of
205 oxygen are marked by in-phase variations of $\delta^{13}\text{C}$ (Fig. 4 and 5). The r^2 values (covariation between
206 $\delta^{18}\text{O}$ and $\delta^{13}\text{C}$ along the growth axis) are 0.33 and 0.36 for D4 and D3 respectively. For the sharp
207 excursion at ca. 132.1 ka, the total $\delta^{13}\text{C}$ change is about 3.6‰. Close to the end of the discussed
208 interval, it is possible to observe a slightly different behavior for the two records: at ca. 126.5 ka the
209 $\delta^{13}\text{C}$ shows the same positive oscillation previously described for the $\delta^{18}\text{O}$ but it is longer and less
210 prominent. After this, the carbon isotopes return to previous values and steadily decrease until
211 hiatus Hs1, whereas the oxygen after ca. 126.5 ka only consistently increases.

212

213 **Discussion**

214 The Tana che Urla proxy record (stable isotope and growth rate, Fig. 5) shows a consistent pattern
215 of variability both at orbital (i.e. glacial-interglacial transition) and suborbital time scales
216 (centennial-to-millennial scale). There is also a persistently good correspondence between the
217 isotopic record (especially for oxygen), growth rate and petrographic change in the cores: the white,
218 clastic-poor calcite occurs during periods of prevailing lower isotope values and higher growth
219 rates, while the brown, clastic-rich calcite occurs principally during periods of lower growth rate
220 and higher isotope values.

221

222 *Equilibrium deposition*

223 In the recent literature, it has been recognized that kinetic isotopic effects are present in many
224 speleothem records (e.g. Mickler et al., 2006; Wainer et al., 2011). “Hendy tests” are the classical
225 tools used to test whether calcite from a given speleothem was deposited out of isotopic equilibrium
226 (Hendy, 1971). We have applied this test to four flowstone laminae to check the isotopic
227 composition behavior laterally. Each case shows no significant correlation between $\delta^{18}\text{O}$ and $\delta^{13}\text{C}$
228 and almost constant values of $\delta^{18}\text{O}$ and $\delta^{13}\text{C}$ along a single growth layers (Fig. 6), suggesting
229 equilibrium or quasi-equilibrium deposition (Hendy, 1971). However, Hendy tests are no longer

230 viewed as definitive proof of isotopic equilibrium (e.g. Mühlhous et al., 2009; Day and
231 Henderson, 2011) and so further evidence of near-equilibrium deposition is required. Recent
232 literature (e.g. Dorale and Liu 2005, Fairchild and Baker, 2012) suggests that near-equilibrium
233 deposition is likely if the isotopic patterns of two or more coeval samples from the same cave
234 reproduce favorably. For the TCU flowstone, comparison between the two stable isotope records of
235 D4 and D3 shows that they are remarkably similar over the contemporaneous growth period,
236 providing a robust replication test (Fig. 4, e.g. Dorale and Liu 2005; Fairchild and Baker, 2012).
237 The small discrepancy between the two records may indicate minor kinetic effects and/or the
238 influence of different growth rates for the two lobes of the flowstone from which the cores were
239 taken, but these differences are small compared to the overall range of values (e.g. for oxygen the
240 biggest excursion corresponding to MIS6/MIS6 transition is from -3.68 to -6.04 ‰ on D4, whereas
241 it is from -2.86 to -6.32 ‰ for D3), suggesting that changes in the $\delta^{18}\text{O}$ are driven by changes in the
242 $\delta^{18}\text{O}$ of meteoric water and cave temperature. Moreover, the monotonous columnar fabric is
243 believed to occur when speleothems are continuously wet, and from fluids at near-isotopic
244 equilibrium conditions with low oversaturation (Frisia et al., 2000).
245 Equilibrium conditions can also be inferred theoretically, in particular using data from modern
246 cave-water monitoring. Water samples collected randomly from several drip sites over three years
247 show average $\delta^{18}\text{O}_w$ values of $-7.13 \pm 0.27\text{‰}$ (n=7). Average $\delta^{18}\text{O}$ values for calcite from the top
248 section of D4 and deposited over the Holocene – a period of relatively little palaeoclimate change -
249 are $-5.23\text{‰} \pm 0.2\text{‰}$. Using the Kim and O'Neil (1997) equation for isotopic fractionation
250 coefficient, we obtain an equilibrium temperature of 7.5°C ($\pm 1.5^\circ\text{C}$), which is somewhat lower than
251 the modern interior cave temperature (10.2°C). However, results from a compilation of published
252 cave monitoring data show a frequent ^{18}O -enrichment of 0.5-1‰ in speleothem calcite compared to
253 the isotopic equilibrium value (McDermott et al., 2006). Although it has yet to be demonstrated that
254 this enrichment is not due to a modest kinetic effect, the temperature inferred for Holocene calcite
255 considering this offset would range from 11.9 and 10.2°C , values which are closer to the modern

256 cave temperature. Although only approximations, these calculations provide additional evidence of
257 ~equilibrium deposition for TCU flowstone.

258 It is possible to estimate the $\delta^{13}\text{C}$ values of speleothem calcite that would have precipitated in
259 equilibrium with seepage waters knowing the $\delta^{13}\text{C}$ values of DIC. The few data available on drips
260 and pool waters from TCU give an average value of $-10.0\pm 1.5\text{‰}$ ($n=4$). Considering the isotopic
261 fractionation factor between CaCO_3 and HCO_3^- of ca. 1‰ (Romanek et al., 1992), calcite
262 precipitated in equilibrium would have values of ca. -9.0‰ , close to observed values for the
263 Holocene ($-9.6\pm 0.3\text{‰}$) and minimum values of the Last Interglacial ($-8.6\pm 0.3\text{‰}$). The small
264 differences can be accounted by a small degree of kinetic isotopic fractionation and/or exchange
265 with cave CO_2 (e.g. Tremaine et al., 2011; Oster et al., 2010). Following the approach of Oster et al.
266 (2010), it is possible to estimate the extent of processes affecting the isotopic composition of the
267 dissolved inorganic carbon of water equilibrated with soil CO_2 and the final carbon isotope
268 composition of speleothem calcite. After equilibration with soil CO_2 , DIC isotopic composition
269 evolves due to the different contributions of bedrock and other processes, such as prior calcite
270 precipitation (e.g. Fairchild et al., 2006 and references therein). In this approach, the isotopic
271 composition of soil litter is assumed to be close to the isotopic composition of soil CO_2 , taking into
272 account fractionation of 4.4‰ caused by differing diffusion coefficients for $^{12}\text{CO}_2$ and $^{13}\text{CO}_2$
273 (Cerling et al., 1991) and a coefficient between HCO_3^- and $\text{CO}_{2(\text{g})}$ of ca. $+9\text{‰}$ (Zhang et al., 1995).
274 Litter samples collected above the cave between 650 to 900 m a.s.l. show average values of -27.4‰
275 $\pm 1.3\text{‰}$ ($n=7$) (Berti, 2010). This allows us to estimate a value of DIC in equilibrium with local soil
276 CO_2 of ca. -13‰ . The ca. 3‰ difference between this value and the DIC measured in the cave can
277 be explained by the contribution from the dissolution of the host bedrock, prior degassing and prior
278 calcite precipitation (Oster et al., 2010) and/or closed-to-open-system evolution of the DIC
279 compared to soil CO_2 and/or mineralization of different organic matter soil components (e.g.
280 Rudzka et al., 2011). Although these calculations can contain large errors, they are consistent with
281 the isotopic composition of the TCU speleothems being close to the water DIC $\delta^{13}\text{C}$ values. This

282 suggests that changes in the $\delta^{13}\text{C}$ values of DIC are mostly related to variations in soil CO_2
283 equilibration.

284 Therefore, there are sufficient arguments to sustain the notion that the isotopic variability observed
285 in the two TCU cores is not dominated by kinetically induced disequilibrium fractionation during
286 calcite precipitation. We thus believe that the TCU isotope time series mainly reflect changes in the
287 $\delta^{18}\text{O}$ of meteoric water and/or cave temperature.

288

289 *Paleohydrological significance of $\delta^{18}\text{O}$ and growth rate*

290 For Mediterranean speleothems, atmospheric condensation temperature effects are likely to be
291 balanced by changes in cave temperature (e.g. Bar-Matthews et al., Bard et al., 2002, Drysdale et al.
292 2004, Zanchetta et al., 2007) and therefore changes in speleothem $\delta^{18}\text{O}$ calcite are thought to reflect
293 principally changes in the isotopic composition of $\delta^{18}\text{O}$ of meteoric precipitation due to the “amount
294 effect” (e.g. Dansgaard et al., 1964) and/or to changes in $\delta^{18}\text{O}$ of ocean surface water (“source
295 effect”) due largely to ice volume changes. This conclusion was first proposed by Bar Matthews et
296 al. (1999, 2000; 2003) for the eastern Mediterranean (Soreq Cave, Israel). Subsequently, it has been
297 suggested that for eastern Mediterranean at glacial/interglacial transition, the influences of rainfall
298 amount, sea–land distance and elevation changes related to sea level changes, are superimposed on
299 ocean-surface water $\delta^{18}\text{O}$ changes, brought about by continental ice melting (Bar-Matthews et al.,
300 2003; Kolodny et al., 2005; Almogi-Labin et al., 2009). Instead, during interglacial periods, the
301 amount effect is considered dominant. On the other hand, for the western Mediterranean, Bard et al.
302 (2002) examined data from the GNIP-IAEA stations of Genoa, Palermo and Pisa and analyzed the
303 inter-annual variations of $\delta^{18}\text{O}_p$ and atmospheric temperature. They showed that $\delta^{18}\text{O}_p$ and
304 temperature are positively correlated, with a slope of $+0.3\text{‰}/^\circ\text{C}$, which is close in magnitude but
305 opposite in sign to the cave-temperature effect ($-0.24\text{‰}/^\circ\text{C}$). More significantly, they found that
306 $\delta^{18}\text{O}_p$ is also anticorrelated with the amount of precipitation, with a slope of -2‰ per 100
307 mm/month. Isotopic modelling performed by Bard et al. (2002) indicated that for the western

308 Mediterranean this effect should be dominant in glacial, interglacial and intermediate climate states.
309 During the deglaciation, the amount effect is clearly superimposed on the effect of changes in the
310 $\delta^{18}\text{O}$ of sea water, both in the Mediterranean and the North Atlantic, which in turns depend on
311 changes in the global ice volume (i.e. lower $\delta^{18}\text{O}$ composition of sea water due to ice melting) as
312 well as on changes in the freshwater budget for Mediterranean, and from evaporation in the tropics
313 and patterns of ocean-water circulation for the North Atlantic (Kallel et al., 2000). Although the
314 relative importance of each effect is difficult to evaluate, they each act in the same direction as the
315 amount effect (i.e. decreasing $\delta^{18}\text{O}$ composition of rainfall during the deglaciation).

316 These considerations have been used to interpret the isotopic records of nearby Corchia Cave (Fig.
317 1), and changes in the amount precipitation inferred from oxygen isotopes from this archive were
318 interpreted due to changes in advection of moisture from Atlantic in response to changes in the
319 strength of MOC (e.g. Drysdale et al., 2004; 2007; Zanchetta et al., 2007). The notion that the $\delta^{18}\text{O}$
320 of speleothem calcite in this area mostly retains information on changes in paleorainfall amount has
321 been supported by trace element and/or growth rate data at Corchia (Drysdale et al., 2009;
322 Regattieri et al., 2014), and Mg and organic fluorescence patterns at the lower-altitude Renella Cave
323 (Drysdale et al., 2006). At Renella Cave, major alluvial phases are in phase with lower $\delta^{18}\text{O}$ values
324 at Corchia during the Holocene (Zhornyak et al., 2011). Thus, it is reasonable to assume that in
325 TCU, speleothem $\delta^{18}\text{O}$ is also mainly driven by the “amount effect” on precipitation related to
326 North Atlantic conditions.

327 The observed variations in the growth rate of the TCU flowstone (Fig. 5) and their potential
328 relationship to hydrological changes should be interpreted with caution because they relate only to
329 one flowstone, and it is reasonable to expect that different parts of the cave may yield differing
330 speleothem growth patterns as fractures widen, narrow, and close over time. However, the changes
331 in growth rate are consistent with the proposed interpretation for stable isotope variations (i.e.
332 higher growth rate during periods of enhanced precipitation), supporting the inferences that they,
333 too, are climate-related.

334

335 *MIS 6 variability and the transition to the Last Interglacial*

336 The basal section of the flowstone, from ca. 158.5 ± 2.7 to 132.2 ± 1.8 ka, shows higher $\delta^{18}\text{O}$ values
337 and lower growth rates (Fig. 5) indicating generally drier conditions. The interval between 160 to
338 130 ka corresponds to late MIS 6, when a large ice sheet covered northern Europe (e.g., Imbrie et
339 al., 1984). This period has been the subject of several studies (e.g. Rossignol-Strick, 1983; 1985;
340 Cheddadi and Rossignol-Strick, 1995; Ayalon et al., 2002, Bard et al., 2002), most of which
341 indicate that conditions through the entirety of MIS 6, even during the coldest events, were
342 relatively humid in comparison to MIS 4-2 (Ayalon et al., 2002). Although resolution and age
343 control through the MIS 6 section of our record inhibits a detailed discussion, it is notable that
344 flowstone growth at TCU during at least the last part of MIS 6 was continuous, whereas the last
345 glacial was characterized by several growth interruptions, suggesting a more severe climate.
346 Furthermore, a prominent phase indicative of enhanced rainfall is centered at ca. 153.1 ± 1.9 ka and
347 also corresponds to a phase of higher growth rate. This excursion lasts ca. 2 ka and terminates quite
348 abruptly. It may correspond to a wetter period identified in Soreq Cave (Israel) speleothems,
349 centered at ca. 152 ka (Aylon et al., 2002). This interval is very prominent in the Soreq Cave record
350 and is thought to correspond to the *G. ruber* $\delta^{18}\text{O}$ minimum from eastern Mediterranean marine
351 cores (e.g., Vergnaud-Grazzini et al., 1977; Bar-Matthews et al., 2003) and to be most probably
352 equivalent to the monsoon index maxima ca. 151 ka (e.g. Melieres et al., 1997). Interestingly, a
353 similar period of enhanced precipitation around 150 ka, indicated by a small $\delta^{18}\text{O}$ anomaly, was
354 recognized also in the speleothem record from Argentarola Cave (Southern Tuscany, Bard et al.,
355 2002), where it was linked to the 150-kyr-BP insolation maximum.

356

357 At ca. 132.1 ± 1.8 ka all speleothem properties show an relatively abrupt and high-amplitude
358 change: oxygen and carbon values decrease rapidly, the growth rates dramatically increase (passing
359 from average values of about 4 mm/kyr to ca. 20 mm/kyr) and the brown, clastic calcite is replaced

360 by the white clastic-poor lithofacies (Regattieri et al., 2012). The $\delta^{18}\text{O}$ record indicates
361 progressively enhanced precipitation over the cave catchment at this time, marking the transition
362 between the penultimate glacial and the last interglacial (i.e. the MIS 6 to MIS 5 transition in
363 marine records). Within age error, the TCU $\delta^{18}\text{O}$ is consistent with the $\delta^{18}\text{O}$ record from Corchia
364 Cave (Drysdale et al., 2005, 2009, Figs 1, 7, 8). Similarities with the oxygen record from Soreq
365 Cave are also evident (Bar-Matthews et al., 2003, Figs 1, 7).
366 Within age error, the TCU record is also in agreement with reconstructions of vegetation changes
367 occurring throughout the deglaciation from marine core MD95-2042 (Iberian margin, southwestern
368 Europe, Sánchez Goñi et al., 1999; 2005, Figs 1, 7), and slightly precedes the glacial-interglacial
369 transition in the Monticchio Lake pollen record (Brauer et al., 2007, Allen et al., 2009, Figs 1, 7).
370 Both pollen records show an increase in woody mesic taxa through the deglacial, which suggests
371 not only wetter but also a warmer climate. This is also supported by alkenone-derived SSTs from
372 marine core ODP-977A (Martrat et al., 2007, Figs 1, 7).

373

374 *Suborbital variability of MIS 5e*

375 The TCU $\delta^{18}\text{O}$ record shows significant multi-centennial variability between the peak interglacial
376 conditions at ca. 131.0 ka and hiatus Hs1 at ca. 121.4 ka. The lowest isotope values occurred
377 between ca. 131.0 and 123.6 ka, indicating that the wettest period lasted ca. 6 ka. However, this
378 period is interrupted by two short prominent events, indicating reduced precipitation between ca.
379 130.7 and 129.6 ka and between ca. 126.7 and 125.6 ka. After 123.6 ka, values again increase
380 abruptly then remain stable until hiatus H1. The regional significance of these events can be
381 evaluated by comparing the TCU record with other archives. The TCU and Corchia records display
382 remarkable similarities also for MIS 5e (Figs 8, 9) whilst an even greater degree of similarity is
383 evident with a speleothem record from western France (Bd-inf, Fig. 9, Bourgeois-Delaunay Cave,
384 Couchoud et al., 2009). The event at ca. 126.7-125.6 ka and another from ca. 123.6 ka to hiatus Hs1
385 are well expressed in all the three records (Fig. 9). Also, cores from two well-studied North Atlantic

386 sites, ODP980 (sub-polar North Atlantic, McManus 1999, 2002, Oppo et al., 2001, 2006; Fig.1) and
387 ODP1059 (Sub-tropical western North Atlantic, Oppo et al., 2001, 2006, Heusser and Oppo, 2003;
388 Fig.1), display two intra-Eemian (or intra-MIS5e) cooling events, labelled C28 and C27 (at ca. 129
389 and 122 ka respectively, Oppo et al., 2001). ODP980 and ODP1059 sites are sensitive to changes in
390 MOC in the North Atlantic Ocean, which in turn affects westward moisture advection and, as
391 previously discussed, precipitation amount in the Mediterranean basin. In these marine cores, the
392 C29 and C28 events slightly follow the glacial termination and thus could be correlated respectively
393 with the event of reduced moisture at ca. 129.6 ka and with that starting at ca. 123.6 ka on D4 $\delta^{18}\text{O}$
394 record. The event at ca. 126.5- 125.6 ka does not seem to have an obvious correlation with sub-
395 polar and western North Atlantic marine cores, although correlation of these events is problematic
396 due to the intrinsically different age models of speleothems and marine cores, and also to the
397 discrepancy in resolution between the different records.

398 Interestingly, the $\delta^{18}\text{O}$ values of TCU after the second event (from ca. 126.5 ka) remain more
399 positive than the early LIG (130-127 ka), thus suggesting that the wettest part of MIS5e in the area
400 occurred in the earliest part of the interglacial.

401 Correlations between two North Atlantic cores (ENAM33 and MD95-2009, Fig.1) from south and
402 north of the Iceland–Scotland Ridge, demonstrate that during the MIS 6/5e transition, the polar
403 front was displaced ca. 1000 km to the southeast compared to the present day, and that sea-surface
404 temperatures rose 3000 years earlier south of the ridge (ca. 130 ka) than north of the ridge (ca. 127
405 ka) (Rasmussen et al., 2003). Whereas NADW formation and, more generally, North Atlantic MOC
406 were not affected by cold surface conditions in the Norwegian Sea before 127 ka, cold surface
407 water conditions in the Nordic seas can be assumed to have had a negative effect on cyclonic
408 activity in this region (Rasmussen et al., 2003). This would imply a reduction of the westerly wind
409 intensity over NW Europe (Rasmussen et al., 2003). For the Holocene, it has been suggested that
410 reduction in the intensity of the westerlies results in increased precipitation over the Mediterranean
411 basin, because the northward transport of vapor masses sourced from the subtropical sector of the

412 North Atlantic is less efficient and therefore part of this moisture can penetrate the basin interior
413 instead of being transferred to NW Europe (Fletcher et al., 2012). We suggest that the apparent
414 reduction in precipitation recorded at TCU (but also in Corchia record, Fig.9) from ca. 127 ka could
415 reflect surface warming of the Nordic seas, producing enhanced cyclonic activity, stronger
416 westerlies and a more efficient transport of vapour masses towards NW Europe. This is supported
417 also by the occurrence of a mid-Eemian wet and cold period in core MD95-2042 around 126.5 ka,
418 so substantially synchronous with the second oxygen depleted event in TCU record, which was
419 presumably related to southward displacement of the Polar Front, favoring the formation of major
420 atmospheric depressions and enhanced cyclonic activity over the North Atlantic and western-
421 southern Europe (Sanchez-Goni et al., 1999).

422

423 *Interpretation of $\delta^{13}C$ record*

424 While the $\delta^{18}O$ signal at Tana che Urla can be linked to regional-scale climatic conditions, the $\delta^{13}C$
425 record gives more detailed information into local environmental changes, even if it strictly follows
426 the $\delta^{18}O$ signal, indicating a strong sensitivity to regional climate change. Interpretations of
427 speleothem $\delta^{13}C$ records are challenging because of the complex reactions involving soil CO_2 ,
428 bedrock dissolution, and the reaction kinetics in the CO_2 - H_2O - $CaCO_3$ system (e.g. Fairchild and
429 Baker, 2012). Many processes, however, tend to drive the final $\delta^{13}C$ of speleothem in the same
430 direction. For instance, elevated values of speleothems can be due to a decrease in soil- CO_2
431 productivity (e.g. Genty et al., 2003), usually associated with a reduction in rainfall and cooler
432 climate. Reduction in recharge can also produce degassing along the fracture paths, with enhanced
433 calcite precipitation occurring before drip waters reach the cave (e.g. Baker et al., 1997; Fairchild et
434 al., 2006). In this view, higher $\delta^{13}C$ values of the calcite between ca. 159 and 132 ka, representing
435 the glacial period of MIS 6, are consistent with a reduction in soil vegetation and respiration rates
436 due to cooling and/or reduced recharge.

437 Regional pollen records for central and Southern Italy (e.g. Follieri et al., 1988; Brauer et al., 2007,
438 Allen et al., 2009) indicate rapid forest expansion at the transition from MIS 6 to MIS 5.
439 Accordingly, the observed $\delta^{13}\text{C}$ variation during the glacial to interglacial transition in TCU is
440 suggests forest expansion, soil development and enhanced soil CO_2 production during the climate
441 transition, leading to a decrease in the speleothem $\delta^{13}\text{C}$. The synchronicity between the $\delta^{18}\text{O}$ and
442 $\delta^{13}\text{C}$ in TCU (Figs 4, 8) indicates that changes in soil conditions in the TCU catchment happened
443 not only relatively quickly but in sync with the increase in rainfall, reaching interglacial values
444 within ca. 2000 years.

445
446 To understand the rapid responses of soil development above TCU Cave, a comparison with the
447 Corchia Cave $\delta^{13}\text{C}$ record for the same interval is useful, and provides insights into the differences
448 in soil evolution above each cave (Fig. 8). At the glacial-interglacial transition, the $\delta^{13}\text{C}$ of Corchia
449 Cave speleothems shows a lagged (ca. 2000 yr) and more gradual shift to lighter values compared
450 to $\delta^{18}\text{O}$, owing to the time required for post-glacial soils to establish above Corchia (Drysdale *et al.*,
451 2004, 2005, 2009; Zanchetta et al., 2007). The present physiographic setting of the two caves is
452 quite different: Corchia Cave is a large (ca. 60 km) and deep (-1187 m below surface) karst system.
453 The recharge area of the well-studied deep chamber “Galleria delle Stalattiti (from where all the
454 published speleothem records are derived so far) is located between 1200 and 1400 m a.s.l. (Piccini
455 et al., 2008) and it is dominated by very steep terrain of mostly bare, high-purity bedrock, with only
456 occasional soil-filled solution features and little vegetation cover. The high $\delta^{13}\text{C}$ values in drip
457 water and speleothems in Corchia (Piccini et al., 2008, Baneschi et al., 2011) suggest a low input of
458 biogenic CO_2 (Dulinski and Rozanski, 1990), having $\delta^{13}\text{C}$ values of DIC of ca. -3.36‰ (SD 0.15‰)
459 (Baneschi et al., 2011). This is in agreement with the poorly developed soil cover and deep location
460 of the chamber, which promotes a greater contribution from bedrock carbon, which has values
461 between -0.5 and $+1.7 \text{‰}$ (range of values for the Grezzoni formation, average $+0.8\pm 0.9 \text{‰}$,
462 Cortecchi et al., 1999). The $\delta^{13}\text{C}$ of soil organic matter collected above Corchia between ca. 1200

463 and 1400 m a.s.l. shows values of $-26.25 \pm 1.54\%$ (Berti, 2010). Performing the same calculation as
464 that for TCU, a DIC in equilibrium with soil CO_2 should have values around -12.85% . The very
465 large difference from this calculated values and the DIC $\delta^{13}\text{C}$ values obtained in the Galleria delle
466 Stalattiti indicate a greater contribution of bedrock (including dissolution due to pyrite weathering,
467 as suggested by chemical mass balance calculations – our unpublished data) and, additionally, other
468 effects like prior calcite precipitation and mixing of solutions having different degrees of evolution
469 (Regattieri et al., 2014). In contrast, Tana che Urla is a small, shallow cave, and the recharge area is
470 covered by a relatively deep soil and sustains a well-developed forest. $\delta^{13}\text{C}$ values in calcite and
471 DIC are very low with respect to Corchia, and, as suggested above, indicate a predominance of a
472 biogenic component in cave water CO_2 and most importantly in the $\delta^{13}\text{C}$ signal of the speleothem.
473 (Fig 8).

474

475 Owing to the present setting of TCU Cave, its continuous speleothem growth during late MIS 6 and
476 the low absolute values of $\delta^{13}\text{C}$ in glacial calcite (even below those of Corchia *interglacial* values),
477 we speculate that soils in the infiltration area of TCU were relatively well developed even during
478 the last part of the penultimate glacial. A certain degree of soil development would allow a rapid
479 recovery of vegetation once climatic amelioration commenced during the glacial-interglacial
480 transition. The simultaneous changes in oxygen and carbon values observed at TCU can also
481 explain the apparent age discrepancies between the TCU and Monticchio records for the LIG: at
482 Lake Monticchio, the transition from the preceding glacial, evident in both the palaeovegetation
483 record and the sediment lithology, began at ca. 130.55 ka BP, extending over a 3.35-kyr period,
484 with the ultimate onset of the interglacial placed at ca. 127.2 ± 1.4 ka (Brauer et al., 2007; Alley et
485 al., 2009). In TCU record, the transition starts at ca. 132.1 ± 1.8 ka (well within age error of
486 Monticchio) and ends at ca. 131.0 ± 1.2 ka, perhaps lasting less than a thousand years. Because of
487 changes in taxa due to plants colonizing from refugia may have a significant inertia, the age offset

488 between the two records for the onset of full interglacial conditions may therefore simply reflect
489 different response times of different proxies (pollen vs. isotopes) to a simultaneous climatic forcing.
490

491 **Conclusions**

492 The growth history and stable isotope geochemistry of two cores from Tana che Urla (Alpi Apuane
493 central-western Italy) preserve a continuous record from the latter part of the penultimate glacial to
494 the middle part of the last interglacial (ca.159-121 ka), and captures both orbital-scale (i.e.
495 glacial/interglacial transition) to sub-orbital climate variability. The most prominent feature of the
496 record is the dramatic excursion toward lower isotope values at ca. 132 ka, coincident with a change
497 in the lithology (from brown, detrital-rich to white, detrital-poor calcite) and a fourfold increase in
498 flowstone growth rate. The shift in all speleothem properties implicates enhanced rainfall in the
499 recharge area, related to climatic amelioration at the glacial/interglacial transition, and agrees
500 (within age errors) with the principal structural features of others speleothem and pollen records
501 from central Italy (Drysedale et al., 2005, 2009; Follieri et al., 1988; Alley et al., 2009; Brauer et al.,
502 2007) as well as with regional SST reconstructions (Martrat et al., 2004, 2007). Interestingly, at
503 TCU the shift in $\delta^{13}\text{C}$ and $\delta^{18}\text{O}$ corresponding to glacial-interglacial transition is substantially
504 synchronous, while at nearby Corchia Cave (Drysedale et al., 2005, 2009; Zanchetta et al., 2007)
505 there is a lag of ca. 2 ka of the shift in $\delta^{13}\text{C}$ with respect to $\delta^{18}\text{O}$. At Corchia Cave, this was
506 interpreted as due to the time lag needed for soil recovering in the high-altitude catchment area (ca.
507 1200 m a.s.l.). Instead, at TCU the contemporaneous decrease in both isotope records suggests that
508 soils in the infiltration area (ca. 600-700 m asl) were relatively well developed even during the last
509 part of the penultimate glacial, allowing a rapid recovery of vegetation once climatic amelioration
510 commenced during the glacial-interglacial transition.

511

512 During late MIS 6, we observe slower growth rates and higher isotope values, suggesting generally
513 cooler-drier conditions, interrupted by a peak towards more negative isotope values and higher

514 growth rates between ca. 154.0 and 151.6 ka. This peak is interpreted as a humid period and is
515 coincident with similar conditions inferred from speleothem records from Israel (Ayalon et al,
516 2002) and southern Tuscany (Bard et al., 2002). Further, the interglacial part of the record shows
517 substantial variability, with three events of reduced moisture at ca. 129.6, 126.0 ka and between
518 123.6 ka and the first growth interruption at ca. 121.4 ka. This climatic instability during the first
519 part of the last interglacial substantially agrees with the nearby speleothem record from Corchia
520 Cave (Drysedale et al., 2005; 2009) and matches the occurrence of cold and dry events recognized in
521 a speleothem record from western France (Couchoud et al., 2009), suggesting a regional expression
522 of these events and firmly anchoring their cause to circulation changes in the adjacent North
523 Atlantic. This idea is further supported by the correlation among the first and the third events
524 recorded at Tana che Urla and two cold events (C28 and C27 at ca. 122 and 129 ka) recorded in
525 North Atlantic marine cores (e.g. Oppo et al, 2001). The second event has no obvious correlation
526 with the North Atlantic record but may coincide with a mid-Eemian cool and wet period identified
527 in the pollen record from marine core MD95-2042 at ca. 126 ka (Sanchez-Goni et al., 1999; 2005),
528 inferred to be due to increased cyclonic activity over western Europe driven by southward
529 displacement of the polar front. The presence of major atmospheric depressions in the sub-polar
530 North Atlantic is thought to be responsible for more efficient vapor-mass transport towards northern
531 and western Europe (Fletcher et al., 2012), leading to less effective penetration of major cyclonic
532 perturbations in the Mediterranean basin and reduced precipitation at TCU.

533

534 **Acknowledgements**

535 Financed by the Australian Research Council Discovery Project scheme (grant number
536 DP110102185). ER is supported by a PhD grant of the School of Graduate Studies Galileo Galilei
537 (University of Pisa). We thank the Federazione Speleologica Toscana and Parco Apuane for
538 supporting our work on Apuan Alps speleothems. We thank I. Baneschi, M. Guidi, C. Boschi and
539 L. Dallai for unpublished isotopic data on Tana Che Urla waters, obtained within collaboration in

540 monitoring cave waters on Apuan Alps. We also thank two anonymous reviewers and the
541 associated editor for their comments and suggestions, which improved the quality of the
542 manuscript.

543

544 **References**

545 Allen, J.R.M., Huntley B. 2009. Last Interglacial palaeovegetation, palaeoenvironments and
546 chronology: a new record from Lago Grande di Monticchio, southern Italy. *Quaternary Science*
547 *Reviews* 28, 1521-1538.

548 Almogi-Labin, A., Bar-Matthews, M., Shriki, D., Kolosovsky, E., Paterne, M., Schilman, B.,
549 Matthews, A. 2009. Climatic variability during the last~ 90ka of the southern and northern
550 Levantine Basin as evident from marine records and speleothems. *Quaternary Science Reviews*, 28,
551 2882-2896.

552 Ayalon, A., Bar-Matthews, M., Kaufman, A. 2002. Climatic conditions during marine isotope stage
553 6 in the eastern Mediterranean region from the isotopic composition of speleothems of Soreq Cave,
554 Israel. *Geology* 30, 303-306.

555 Baker, A., Barnes, W.L., Smart, P.L., 1997. Variations in the discharge and organic matter content
556 of stalagmite drip waters in Lower Cave, Bristol. *Hydrological Processes* 11, 541-555.

557 Baneschi, I., Piccini, L., Regattieri, E., Isola, I., Guidi, M., Lotti, L., Mantelli, F., Menichetti, M.,
558 Drysdale, R.N., Zanchetta, G. 2011. Hypogean microclimatology and hydrology of the 800-900 m
559 a.s.l. level in the Monte Corchia Cave (Tuscany, Italy): Preliminary considerations and implications
560 for paleoclimatological studies. *Acta Carsologica* 40,175-187.

561 Bard, E., Delaygue, G., Rostek, F., Antonioli, F., Silenzi, S., Schrag, D.P. 2002. Hydrological
562 conditions over the western Mediterranean basin during the deposition of the cold Sapropel 6 (ca.
563 175 kyr BP. *Earth and Planetary Science Letters* 202, 481-494.

564 Bar-Matthews, M., Ayalon, A., Kaufman, A., Wasserburg, G.J. 1999. The Eastern Mediterranean
565 paleoclimate as a reflection of regional events: Soreq Cave, Israel. *Earth Planetary Science Letters*
566 166, 85-95.

567 Bar-Matthews, M., Ayalon, A., Kaufmann, A. 2000. Timing and hydrological conditions of
568 sapropel events in the eastern Mediterranean, as evident from speleothems, Soreq Cave, Israel.
569 *Chemical Geology* 169, 145-156.

570 Bar-Matthews, M., Ayalon, A., Gilmour, M. 2003. Sea-land oxygen isotopic relationships from
571 planktonic foraminifera and speleothems in the Eastern Mediterranean region and their implication
572 for paleorainfall during interglacial intervals. *Geochimica et Cosmochimica Acta* 67, 3181-3199.

573 Berger, A., and Loutre, M. F. 1991. Insolation values for the climate of the last 10 million years.
574 *Quaternary Science Reviews*, 10, 297-317.

575 Berti, F. 2010. Studio geochimico ed isotopico di suoli delle Alpi Apuane: Implicazioni per le
576 ricostruzioni climatiche e paleoclimatiche. Master Thesis on Natural Sciences, University of Pisa,
577 1-115.

578 Bond, G., Showers, W., Cheseby, M., Lotti, R., Almasi, P., De Menocal, P., Priore, P., Cullen, H.,
579 Hajdas, I., Bonani, G. 1997. A pervasive millennial-scale cycle in the North Atlantic Holocene and
580 glacial climates. *Science* 294, 2130-2136.

581 Bond, G., Kromer, B., Beer, J., Muscheler, R., Evans M.N., Showers W., Hoffman S., Lotti-Bond,
582 R., Hajadas, I., Bonani G. 2001. Persistent solar influence on North Atlantic climate during
583 Holocene. *Science* 7, 2130-2136.

584 Brauer, A., Allen, J.R.M., Mingram, J., Dulski, P., Wulf, S., Huntley, B. 2007. Evidence for the last
585 interglacial chronology and environmental change from Southern Europe. *Proceeding of the*
586 *National Academy of Science USA* 104, 450-455.

587 Broecker, W.S., Denton, G.H., 1990. The role of ocean-atmosphere reorganizations in glacial
588 cycles. *Quaternary Science. Reviews* 9, 305-341.

589 Broecker, W., Henderson, G. 1998. The sequence of events surrounding Termination II and their
590 implications for the cause of glacial–interglacial CO₂ changes. *Paleoceanography* 13, 352-364.

591 Cerling, T.E., Solomon, D.K., Quade, J., Bowman, J.R. 1991 On the isotopic composition of carbon
592 in soil carbon dioxide. *Geochimica et Cosmochimica Acta* 55, 3404-3405.

593 Cheddadi, R., and Rossignol-Strick, M., 1995, Eastern Mediterranean Quaternary paleoclimates
594 from pollen and isotope records of marine cores in the Nile cone area. *Paleoceanography* 10, 291-
595 300.

596 Couchoud, I., Genty, D., Hoffmann, D., Drysdale, R.N., Blamart, D. 2009. Millennial-scale
597 variability during the Last Interglacial recorded in a speleothem from south-western France.
598 *Quaternary Science Review* 28, 3263-3274.

599 Dansgaard W. 1964. Stable isotopes in precipitation, *Tellus* 16, 436-468.

600 Dulinski, M., Rozanski, K. 1990. Formation of C-13 C-12 isotope ratios In speleothems-A
601 semidynamic model. *Radiocarbon* 32, 7-16.

602 Day, C.C., Henderson, G.M. Oxygen isotopes in calcite under cave-analogue conditions.
603 *Geochimica et Cosmochimica Acta* 75, 3956-3972.

604 Dorale, A., Liu, Z. 2005. Limitations of hendi test criteria in judging the paleoclimatic suitability of
605 speleothems and the need for replication. *Journal of Cave and Karst Studies* 71, 73–80.

606 Drysdale, R.N., Zanchetta, G., Hellstrom, J.C., Fallick, A.E., Zhao, J.X., Isola, I., Bruschi, G. 2004.
607 Palaeoclimatic implications of the growth history and stable isotope ($\delta^{18}\text{O}$ and $\delta^{13}\text{C}$) geochemistry
608 of a Middle to Late Pleistocene stalagmite from central-western Italy. *Earth and Planetary Science*
609 *Letters* 227, 215-229.

610 Drysdale, R.N., Zanchetta, G., Hellstrom, J.C., Fallick, A.E., Zhao, J.X. 2005. Stalagmite evidence
611 for the onset of the Last Interglacial in southern Europe at 129+/-1 ka. *Geophysical Research*
612 *Letters* 32, 1-4.

613 Drysdale, R.N., Zanchetta, G., Hellstrom, J.C., Maas, R., Fallick, A.E., Pickett, M., Cartwright, I.,
614 Piccini, L. 2006. Late Holocene drought responsible for the collapse of Old World civilizations is
615 recorded in an Italian cave flowstone. *Geology* 34, 101-104.

616 Drysdale, R.N., Zanchetta, G., Hellstrom, J.C., Fallick, A.E., McDonald, J., Cartwright, I. 2007.
617 Stalagmite evidence for the precise timing of North Atlantic cold events during the early last
618 glacial. *Geology* 35, 77-80.

619 Drysdale, R.N., Zanchetta, G., Hellstrom, J.C., Fallick, A.E., Sanchez-Goni, M.F., Couchoud, I.,
620 McDonald, J., Maas, R., Lohmann, G., Isola, I. 2009. Evidence for obliquity forcing of glacial
621 termination II. *Science* 325, 1527-1531.

622 Fairchild, I.J., Smith, C.L., Baker, A., Fuller, L., Spotl, C., Matthey, D., McDermott, F., E.I.M.F.
623 2006. Modification and preservation of environmental signals in speleothems. *Earth-Science*
624 *Review* 75 : 105-153.

625 Fairchild, I.J., Baker, A. 2012 *Speleothem Science- From processes to past environments.*
626 *Quaternary Geosciences Series.*Wiley-Blakwell : 3-370.

627 Fletcher, W.J., Debret, M., Sanchez-Goni, MF. 2012. Mid-Holocene emergence of a low frequency
628 millennial oscillation in western Mediterranean climate: implications for past dynamics of the North
629 Atlantic atmospheric westerlies. *The Holocene* 0, 1-14

630 Follieri, M., Magri, D., Sadori, L. 1988. 250,000-year pollen record from Valle di Castiglione
631 (Roma). *Pollen et Spores* 30,329-356.

632 Frisia, S. Borsato, A., Fairchild, I.J., McDermott, F. 2000. Calcite fabrics, growth mechanisms and
633 environments of formation in speleothems from the Italian Alps and southwestern Ireland. *Journal*
634 *of Sedimentary Petrology* 70, 1183-1196.

635 Genty D., Blamart D., Ouahdi, R., Gilmour, M., Baker A., Jouzel J., Van-Exter, S. 2001. Precise
636 dating of Dansgaard–Oeschger climate oscillations in western Europe from stalagmite data. *Nature*
637 421, 833-837.

638 Hellstrom, J.C. 2003. Rapid and accurate U/Th dating using parallel ion-counting multicollector
639 ICP-MS. *Journal of Analytical Atomic Spectrometry* 18, 1346-1351.

640 Hellstrom, J.C. 2006. U–Th dating of speleothems with high initial ^{230}Th using stratigraphical
641 constraint. *Quaternary Geochronology* 1, 289-295.

642 Hendy, C.H. 1971. The calculation of the effects of different modes of formation on the isotopic
643 composition of speleothems and their applicability as palaeoclimatic indicators. *Geochimica et*
644 *Cosmochimica Acta* 35, 801-824.

645 Heusser, L., Oppo, D. 2003. Millennial- and orbital-scale climate variability in south-eastern United
646 States and in the subtropical Atlantic during Marine Isotope Stage 5: evidence from pollen and
647 isotopes in ODP Site 1059. *Earth and Planetary Science Letters* 214, 483-490.

648 Imbrie, J., Hays, J.D., Martinson, D.G., McIntyre, A., Mix, A.C.; Morley, J.J.; Pisias, N.G., Prell,
649 W.L. 1984. The orbital theory of Pleistocene climate: support from a revised chronology of the
650 marine $\delta^{18}\text{O}$ record. *Milankovitch and Climate: Understanding the Response to Astronomical*
651 *Forcing*, Proceedings of the NATO Advanced Research Workshop, p. 269.

652 Kim, S.T., O'Neill, J.R. 1997. Equilibrium and non-equilibrium oxygen isotope effects in synthetic
653 carbonates. *Geochimica et Cosmochimica Acta* 61, 3461-3475.

654 Kolodny, Y., Stein, M., & Machlus, M. 2005. Sea-rain-lake relation in the Last Glacial East
655 Mediterranean revealed by $\delta^{18}\text{O}$ - $\delta^{13}\text{C}$ in Lake Lisan aragonites. *Geochimica et Cosmochimica Acta*,
656 69, 4045-4060.

657 Kukla, G., Mcmanus, J.F., Rousseau, D.D., Chuine, I. 1997. How long and how stable was the Last
658 Interglacial?. *Quaternary Science Reviews* 16, 605-612.

659 Kukla, G.J, Bender, M.L., de Beaulieu J.L., Bond, G., W.S., Cleveringa, P., Gavin, J.E., Herbert,
660 T.D., Imbrie, J., Jouzel, J., L.D., Knudsen, K.L., McManus, J.F., Merkt, J., Muhs, D.R. Muller, H.,
661 Poore, R., Z., Porter, S.C., Seret, G., Shackleton, N.J., Turner, C., Tzedakis, P.C., Winograd, I.J.
662 2002. Last Interglacial Climates. *Quaternary Research* 58, 2-13.

663 Lezine, A.M., Von Grafenstein U., Andersen, N., Belmecheri, S., Bordon, A., Caron, B., Cazet J.P.,
664 Erlenkeuser, H., Fouached, E., Grenier, C., Huntsman-Mapila, P., Hureau-Mazaudier, D., Manelli,
665 D., Mazaud, A., Robert, C., Sulpizio, R., Tiercelin, J.J., Zanchetta, G., Zeqollari, Z. 2010. Lake
666 Ohrid, Albania, provides an exceptional multi-proxy record of environmental changes during the
667 last glacial–interglacial cycle. 287, 116-127.

668 Martrat, B., Grimalt, J.O., Lopez-Martinez, C., Chaco, I., Sierro, F.J., Flores, J.A., Zahn, R., Canals,
669 M., Jason, H.C., Hodell, D.A. 2004. Abrupt temperature changes in the Western Mediterranean
670 over the past 250,000 years. *Science* 306, 1762-1765.

671 Martrat B., Grimalt J.O., Shackleton N.J. Deabreu L., Hutterly M.A., Stocker T.F.; 2007- *Four*
672 *climate cycles of recurring deep and surface water destabilizations on the Iberian Margin-* *Science*
673 317 (5837), 502–507

674 McDermott, F., Schwarcz, H., Rowe, J.P. 2006 Isotopes in speleothemes. *Isotopes in*
675 *Paleoenvironmental Research*, E. by Leng M.J, vol 10,185-218.

676 McManus, J.F., Bond, G.C., Broecker, W.S., Johnsen, S., Labeyrie, L., Higgins, S. 1994. High-
677 resolution climate records from the North Atlantic during the last interglacial. *Nature* 371, 326-329.

678 McManus, J.F., Oppo, D.W., Cullen, J.L., 1999. A 0.5-million-year record of millennial-scale
679 climate variability in the North Atlantic. *Science* 283, 971-975.

680 McManus, J.F., Oppo, D.W., Keigwin L.D., Cullen, J.L.; Bond G.C. 2002. Thermohaline
681 Circulation and Prolonged Interglacial Warmth in the North Atlantic. *Quaternary Research* 58, 17-
682 21.

683 Mélières, M.A., Rossignol-Strick, M., Malaize, B.. 1997. Relation between low latitude insolation
684 and $\delta^{18}\text{O}$ change of atmospheric oxygen for the last 200 kyrs, as revealed by Mediterranean
685 sapropels: *Geophysical Research Letters* 24, 1235–1238.

686 Mickler, P.J., Stern, L.A., Banner J.L. 2006. Large kinetic isotope effects in modern speleothems
687 *GSA Bulletin* 118, 65-81.

688 Mühlinghaus, C., Scholz, D., Mangini, A. 2009. Modelling fractionation of stable isotopes in
689 stalagmites, *Geochimica et Cosmochimica Acta*, 73, 7275-7289.

690 Mussi, M., Leone, G., Nardi, I. 1998. Isotopic composition of natural waters from the Alpi Apuane-
691 Garfagnana area, northern Tuscany, Italy. *Mineralogica Petrographica Acta* 41, 163-178.

692 Oppo, D.W., Lehmann, S.J., 1995. Suborbital timescale variability of North Atlantic Deep Water
693 during the past 200,000 years. *Paleoceanography* 10, 901-910.

694 Oppo, D.W., Keigwin, L.D., McManus J.F. 2001. Persistent suborbital climate variability in marine
695 isotope stage 5 and Termination II. *Paleoceanography* 16, 280-292.

696 Oppo, D.W., McManus, J.F., Cullen, J.L. 2006. Evolution and demise of the Last Interglacial
697 warmth in the subpolar North Atlantic. *Quaternary Science Reviews* 25, 3268-3277.

698 Oster, J.L., Montanez, I.P., Guilderson, T.P., Sharp, W.D., Banner, J.L. 2010. Modeling speleothem
699 $\delta^{13}\text{C}$ variability in a central Sierra Nevada cave using ^{14}C and $^{87}\text{Sr}/^{86}\text{Sr}$. *Geochimica et*
700 *Cosmochimica Acta* 74, 5228-5242.

701 Pandeli, E., Bagnoli, P., Negri, M. 2004. The Fornovolasco schists of the Apuan Alps (Northern
702 Tuscany, Italy): a new hypothesis for their stratigraphic setting. *Bollettino Società Geologica* 123,
703 53-66.

704 Piccini, L., Pranzini, G., Tedici L., Forti, P. 1999. Le risorse idriche dei complessi carbonatici del
705 comprensorio apuo-versiliese. *Quaderni di Geologia Applicata* 6, 61-78.

706 Piccini, L., Zanchetta, G., Drysdale, R.N., Hellstrom, J.C., Isola, I., Fallick, A.E., Leone, G.,
707 Doveri, M., Mussi, M., Mantelli, F., Molli, G., Lotti, L., Roncioni, A., Regattieri, E., Meccheri, M.,
708 Vaselli, L. 2008. The environmental features of the Monte Corchia cave system (Apuan Alps,
709 central Italy) and their effects on speleothem growth. *International Journal of Speleology* 37, 153-
710 172

711 Rahmstorf, S. 1995. Bifurcations of the Atlantic thermohaline circulation in response to changes in
712 the hydrological cycle. *Nature* 378, 145-149.

713 Rasmussen, T.L., Thomsen, E., Kuijpers, A., Wastegård, S., 2003. Late warming and early cooling
714 of the sea surface in the Nordic seas during MIS 5e (Eemian Interglacial) *Quaternary Science*
715 *Reviews* 22, 809-821.

716 Regattieri, E., Isola, I., Zanchetta, G, Drysdale, R.N., Hellstrom, J.C., Baneschi, I. 2012.
717 Stratigraphy, petrography and chronology of speleothem deposition at Tana che Urla (Lucca, Italy):
718 paleoclimatic implications. *Geografia Fisica e Dinamica del Quaternario* 35, 141-152.

719 Regattieri, E., Zanchetta, G., Drysdale, R.N., Isola, I., Hellstrom, J.C., Dallai, L.. 2014. Late-glacial
720 to Holocene trace element record (Ba, Mg, Sr) from Corchia Cave (Apuan Alps, central Italy):
721 paleoenvironmental implications. *Journal of Quaternary Sciences* 29, 381–392.

722 Richards, D.A., Dorale, J.A., 2003. Uranium-series chronology and environmental applications of
723 speleothems. *Reviews in Mineralogy and Geochemistry* 52, 407– 460.

724 Romanek, C.S., Grossman, E.L., Morse, J.W. 1992. Carbon isotopic fractionation in synthetic
725 aragonite and calcite: Effects of temperature and precipitation rate. *Geochimica et Cosmochimica*
726 *Acta* 56, 419-430.

727 Rossignol-Strick, M., 1983. African monsoons, as immediate climate response to orbital insolation:
728 *Nature* 304, 46–48.

729 Rossignol-Strick, M.. 1985. Mediterranean Quaternary sapropels, an immediate response of the
730 African monsoon to variation of insolation: Palaeogeography, Palaeoclimatology, Palaeoecology
731 49, 237–263.

732 Ruddiman, W.F., McIntyre, A., 1976. Northeast Atlantic paleoclimatic changes over the past
733 600,000 years. *Geol. Soc. Am. Mem.* 145, 155-173.

734 Rudzka, D., McDemott, F.; Baldini, L.M., Fleitmann, D., Moreno, A., Stoll, H. 2011. The coupled
735 $\delta^{13}\text{C}$ -radiocarbon systematics of three Late Glacial/early Holocene speleothems; insights into soil
736 and cave processes at climatic transitions. *Geochimica et Cosmochimica Acta* 75, 4321-4339.

737 Sánchez Gōni, M.E., Turon, J.-L., Eynaud F., Shackleton, N.J., 1999. High resolution palynological
738 record off the Iberian margin: direct land-sea correlation for the Last Interglacial complex. *Earth*
739 *and Planetary Science Letters* 171, 123–137. 1999.

740 Sanchez-Goni, M.F. 2005- Introduction to Climate and Vegetation in Europe during MIS5. In *The*
741 *Climate of the Past Interglacial. Developments in Quaternary Science* 7, 197-205.

742 Sprovieri, R., Di Stefano, E., Incarbona, A., Oppo, D.W. 2006. Suborbital climate variability during
743 Marine Isotopic Stage 5 in the central Mediterranean basin: evidence from calcareous plankton
744 record. *Quaternary Science Reviews* 25, 2332-2342.

745 Tremaine, D.M., Froelich, P.N., Wang, Y. 2011. Speleothem calcite farmed in situ: Modern
746 calibration of $\delta^{18}\text{O}$ and $\delta^{13}\text{C}$ paleoclimate proxies in a continuously-monitored natural cave system.
747 *Geochimica et Cosmochimica Acta* 75, 4929-4950.

748 Tzedakis P.C., Raynaud, D., McManus J.F., Berger, A., Brovkin V., Kiefer, T. 2009. Interglacial
749 diversity. *Nature Geoscience* 2, 751-755.

750 Vergnaud-Grazzini, C., Ryan, W.B.F., Cita, M.B. 1977. Stable isotope fractionation, climate change
751 and episodic stagnation in the Eastern Mediterranean during the late Quaternary. *Marine*
752 *Micropaleontology* 2, 353-370.

753 Vogel, H., Zanchetta, G., Sulpizio, R., Wagner B., Nowaczyk N. 2009. A tephrostratigraphic
754 record for the last glacial-interglacial cycle from Lake Ohrid, Albania and Macedonia. *Journal of*
755 *Quaternary Science* 25, 320-338.

756 Wanner, H., Brönnimann, S., Casty, C., Gyalistras, D., Luterbacher, J., Stephenson, D., Xoplaki,
757 E. 2001. North Atlantic Oscillation. Concepts and studies. *Surveys Geophysics* 22, 321-381.

758 Wainer, K., Genty, D., Daeron, M., Bar-Matthews, M., Vonhof, H., Dublyansky, Y., Pons-Branchu,
759 E., Thoma, L., van Calsteren, P., Quiunif, Y., Caillon, N. 2011. Speleothem record of the last 180
760 ka in Villars cave (SW France): Investigation of a large $\delta^{18}\text{O}$ shift between MIS6 and MIS5.
761 *Quaternary Science Reviews*, 30, 130-146.

762 Zanchetta, G., Drysdale, R.N., Hellstrom, J.C., Fallick, A.E., Isola, I., Gagan, M., Pareschi, M.T.
763 2007. Enhanced rainfall in the western Mediterranean during deposition of sapropel S1: stalagmite
764 evidence from Corchia Cave (Central Italy). *Quaternary Science Reviews* 26, 279-286.

765 Zhang, J., Quay, P.D., Wilbur D.O. 1995. Carbon isotope fractionation during gas-water exchange
766 and dissolution of CO₂. *Geochimica et Cosmochimica Acta* 59, 107-114.

767 Zhornyak, L.V., Zanchetta, G., Drysdale, R.N., Hellstrom, J.C., Isola, I., Regattieri, E., Piccini, L.,
768 Baneschi, I., Couchoud, I. 2011. Stratigraphic evidence for a “pluvial phase” between ca 8200 and
769 7100 ka from Renella cave (Central Italy). *Quaternary Science Reviews* 30, 409-417.

770

771 **Table and Figures captions**

772 Table1-Corrected U/Th ages for TCU D3 and TCU D4 cores. The activity ratios have been
773 standardized to the HU-1 secular equilibrium standard, and ages calculated using decay constants of
774 9.195×10^{-6} (²³⁰Th) and 2.835×10^{-6} (²³⁴U). Depths are from top, whilst the numbers in brackets are
775 the 95% uncertainties.

776 Figure 1 - Top: location of the Apuan Alps and other sites mentioned in the text; Bottom: simplified
777 geology of the Apuan Alps showing main peaks and locations of Tana che Urla, Corchia and
778 Renella Caves.

779 Figure 2 – Middle: TCU cores D3 (top) and D3 (bottom), showing stratigraphic correlations and
780 main lithofacies (in grey) from Regattieri et al. (2012). Top (D3) and bottom (D4): ages vs. depth
781 (mm from top). ‘Hs1’ is the hiatus, which marks the end of the discussed section – see main text for
782 details.

783 Figure 3 - Depth-age model (depth from core top in mm) for the discussed section of continuous
784 growth of core D4. The outer shaded zones define the 95% uncertainties.

785 Figure 4 - Stable isotope compositions and lithofacies (from Regattieri et al., 2012) vs. depth from
786 top (mm) of cores D3 (top) and D4 (bottom) ($\delta^{13}\text{C}$ in red, $\delta^{18}\text{O}$ in blue). Black line marks the hiatus
787 Hs1 and shaded area highlights the excursion corresponding to glacial/interglacial transition. See
788 main text for details.

789 Figure 5 - Stable isotope and growth rate time series for the ca. 159 - 121 ka section of core D4. The
790 growth rate time series is derived from age-depth modelling (see Hellstrom et al., 2006), the
791 envelope represents the 2σ uncertainties.

792 Figure 6 - Results of Hendy tests performed on core D4. Right panel: $\delta^{13}\text{C}$ in grey, $\delta^{18}\text{O}$ in black.

793 Figure 7 - Comparison between $\delta^{18}\text{O}$ of core D4 (a) and $\delta^{18}\text{O}$ of Corchia Cave (b), stalagmites CC5
794 blue, CC7 light blue, (Drysedale et al., 2009), $\delta^{18}\text{O}$ of Soreq Cave (c, Bar-Matthews et al., 2003),
795 percentage of arboreal pollen at lake Monticchio (d, Brauer et al., 2007, Allen et al., 2009).
796 percentage of warm and temperate species from Iberian-margin marine core MD95-2042 (e,
797 Sanchez-Goni et al., 1999, 2005), alkenone-based sea-surface temperatures from western
798 Mediterranean core ODP-977A (f, Martrat et al., 2004) and June insolation at 65°N (g, Berger and
799 Loutre, 1991). All records are reported on their own published age models. Grey shading highlights
800 the outer range of the excursion corresponding to glacial-interglacial transition.

801 Figure 8 - Comparison of $\delta^{18}\text{O}$ and $\delta^{13}\text{C}$ between TCU core D4 and Corchia Cave (stalagmite CC5,
802 Drysdale et al., 2005; 2009).

803 Figure 9 - Comparison of MIS5e variability from $\delta^{18}\text{O}$ of core D4, $\delta^{18}\text{O}$ of stalagmite BD-inf
804 (Bourges-Delauny Cave, Couchoud et al., 2009) and $\delta^{18}\text{O}$ of Corchia Cave (stalagmites CC5 blue
805 and CC7 light-blue, Drysdale et al., 2005; 2009). Grey shading indicates drier intervals from D4
806 record, grey dashed lines indicate C28 and C29 cold events from Oppo et al. (2001) and the middle-
807 Eemian cooling event from marine core MD95-2042 (Sanchez-Goni et al., 1999, 2007).

808

809

810

Table 1

Sample ID	^{238}U ng/g	Depth/mm	$(^{230}\text{Th}/^{238}\text{U})$	$(^{234}\text{U}/^{238}\text{U})$	$(^{232}\text{Th}/^{238}\text{U}) * 1000$	$^{230}\text{Th}/^{232}\text{Th}$	Age Ka	2se
TCUD4-D	30	9.1	0.10	1.35	3.91	26.18	7.79	(0.28)
TCUD4-24.5	25	24.5	0.17	1.33	9.75	17.15	12.61	(0.65)
TCUD4-46.5	29	46.5	0.66	1.28	5.91	111.43	75.03	(0.78)
TCUD4-70.5	25	70.5	0.72	1.27	31.77	22.59	81.12	(2.61)
TCUD4-77.5	25	77.5	0.72	1.24	48.35	14.86	80.52	(3.56)
TCUD4-90.5	18	90.5	0.84	1.24	30.71	27.48	112.55	(2.77)
TCUD4-102.5A	21	102.5	0.91	1.24	70.09	12.97	120.44	(5.36)
TCUD4-102.5B	18	102	0.91	1.24	62.34	14.57	122.15	(4.68)
TCUD4-C	42	123.5	0.81	1.16	6.19	131.25	124.30	(1.16)
TCUD4-4	52	156.5	0.87	1.22	5.96	146.66	128.10	(1.98)
TCUD4-181.5	41	181.5	0.88	1.22	5.60	156.71	129.24	(1.98)
TCUD4-B	64	207.5	0.88	1.23	7.11	124.47	129.21	(1.10)
TCUD4-212.5	34	212.5	0.90	1.23	6.82	132.55	133.73	(2.17)
TCUD4-3	50	225.5	0.91	1.24	17.07	53.15	131.23	(2.01)
TCUD4-244.5	43	244.5	0.93	1.23	30.38	30.73	139.44	(2.89)
TCUD4-263.5	43	263.5	0.95	1.22	27.60	34.37	146.38	(2.91)
TCUD4-2	71	287.5	0.95	1.20	22.75	41.79	155.30	(3.12)
TCUD4-1	52	309.5	0.95	1.20	18.67	50.65	152.83	(2.94)
TCUD4-A	54	334.5	0.94	1.18	6.01	155.79	159.08	(2.41)
TCU D3 A_d	27	28.5	0.67	1.28	0.23	0.23	43.37	(41.35)
TCU D3 Abis C	42	190.0	1.06	1.26	0.25	0.25	99.26	(21.38)
TCU D3 Abis.b	35	281.0	0.76	1.22	0.01	0.01	100.25	(2.97)
TCU D3 E	36	313.0	0.89	1.19	0.10	0.10	111.826	(5.50)
TCU D3 C	89	458.5	0.91	1.21	0.08	0.08	119.164	(4.16)
TCU.D3 B_e	74	509.5	0.98	1.22	0.07	0.07	144.10	(3.98)

Figure 1
[Click here to download high resolution image](#)

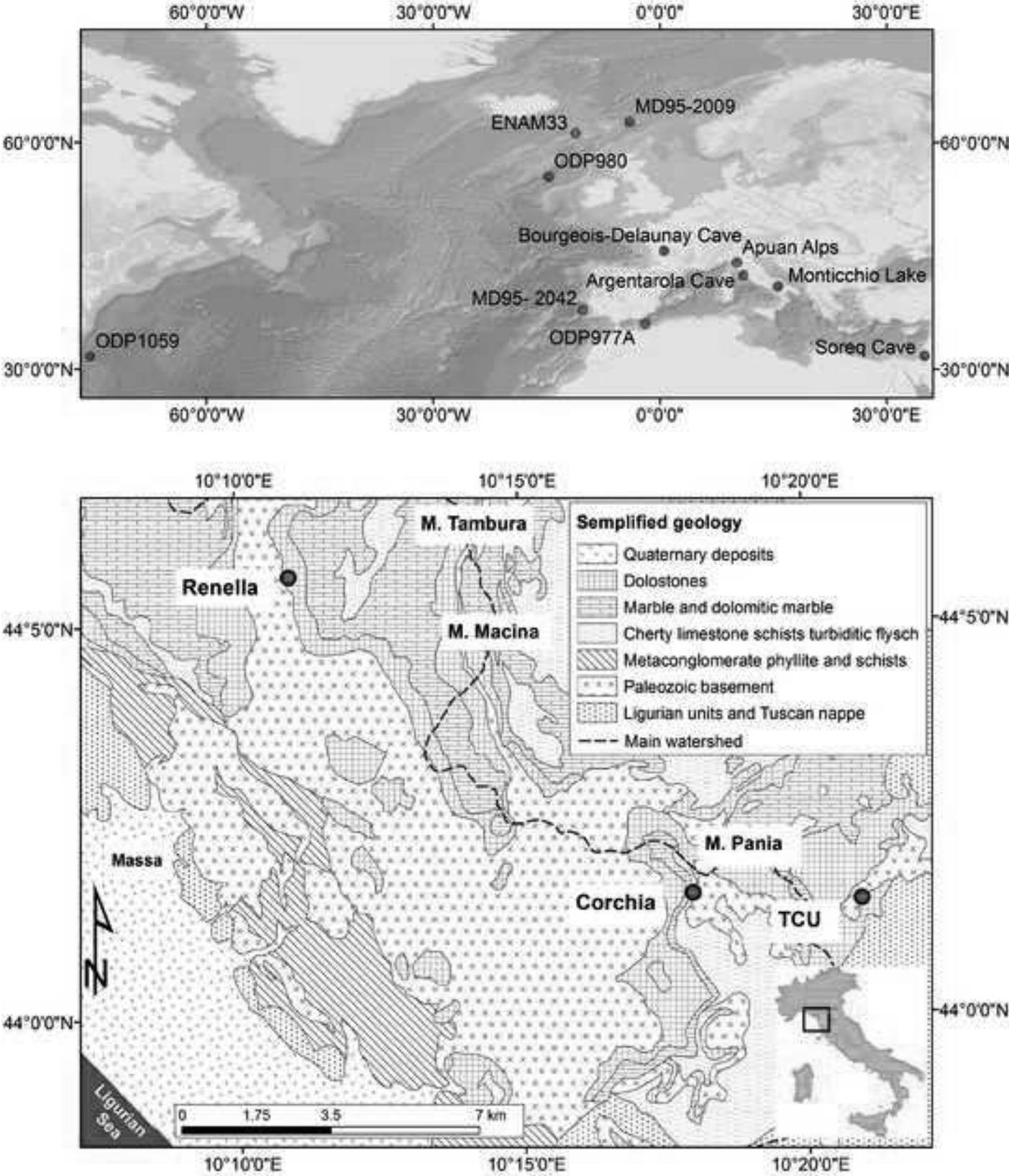


Figure 3
[Click here to download high resolution image](#)

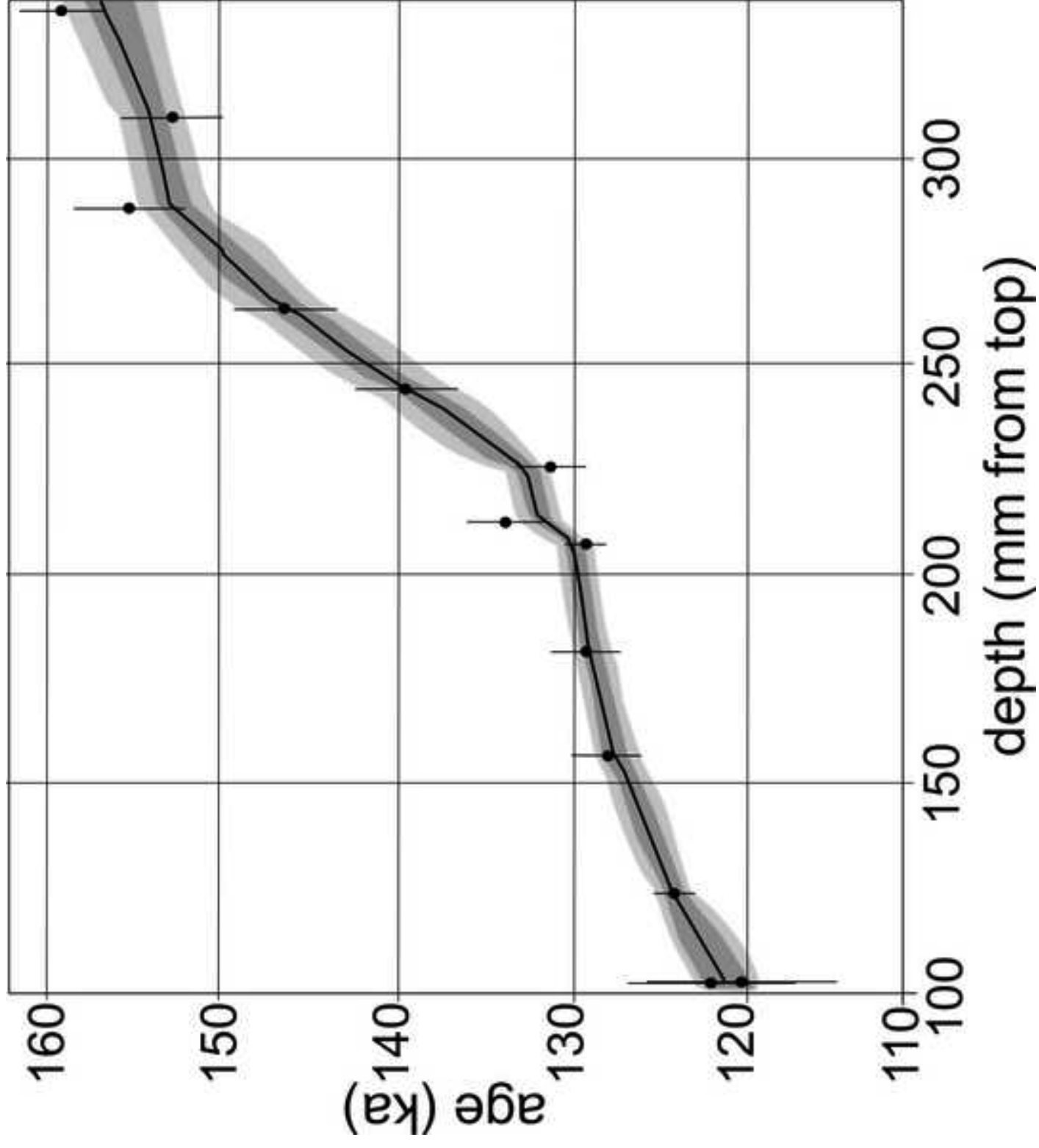


Figure 4
Click here to download high resolution image

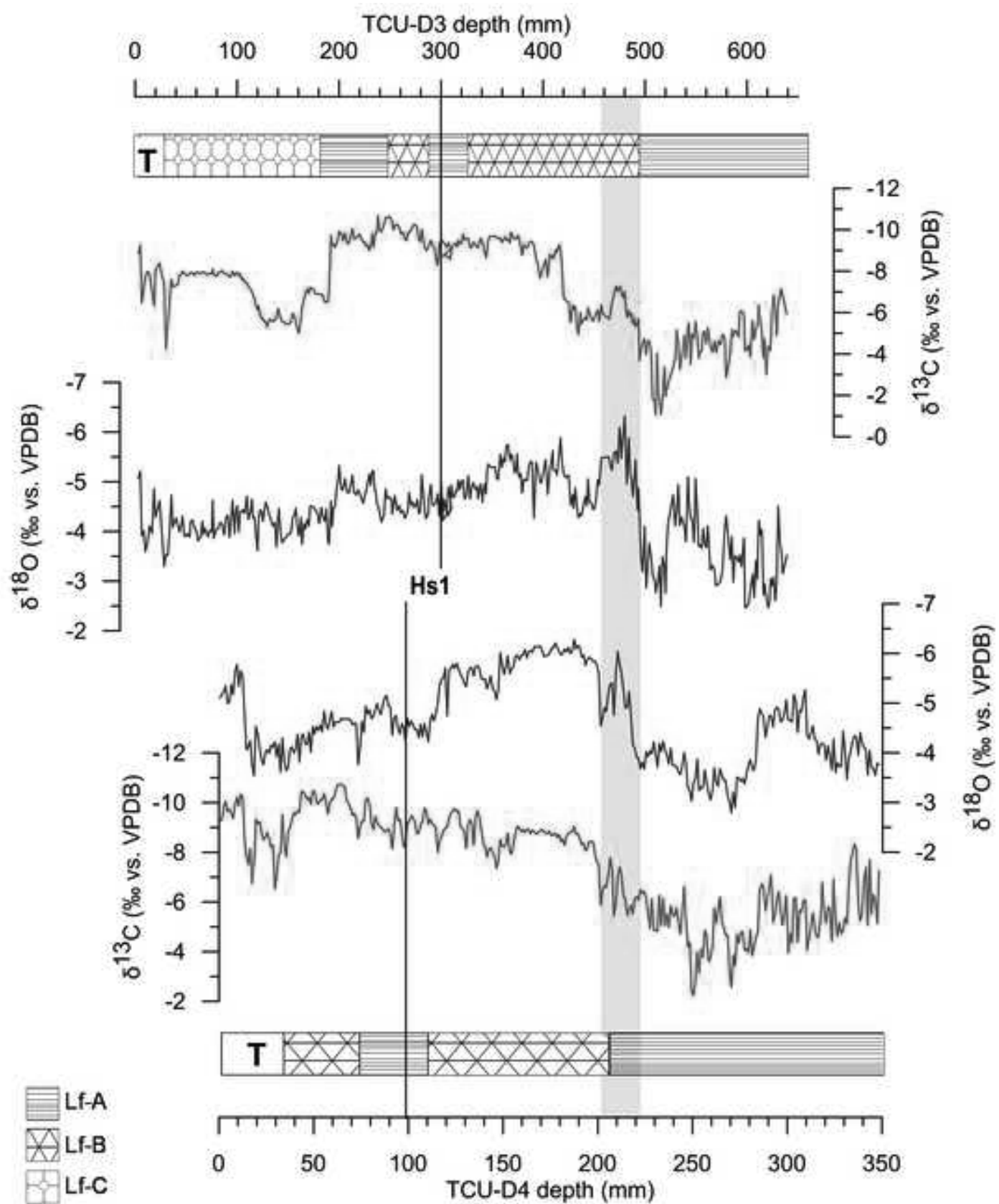


Figure 5
[Click here to download high resolution image](#)

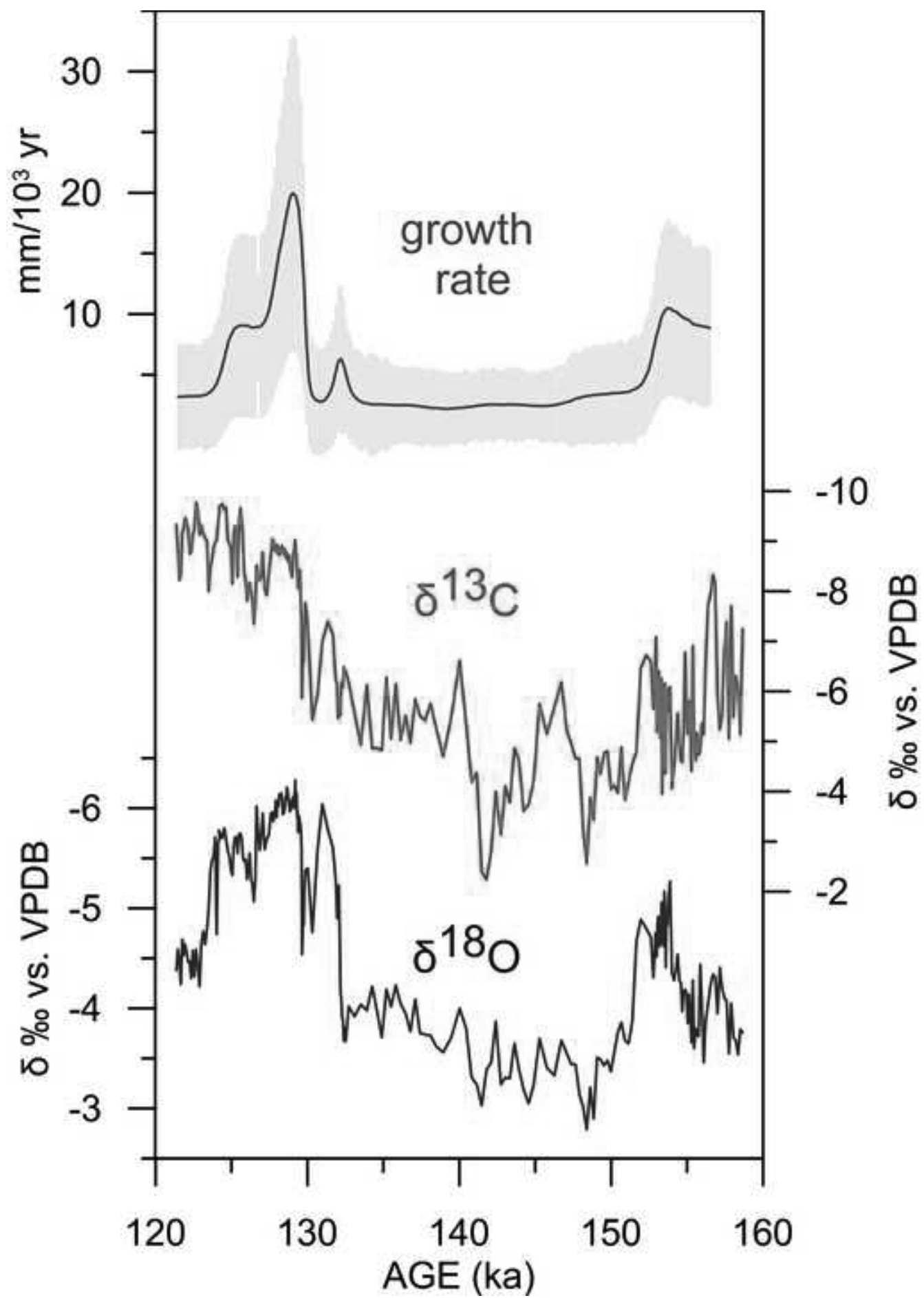


Figure 6
Click here to download high resolution image

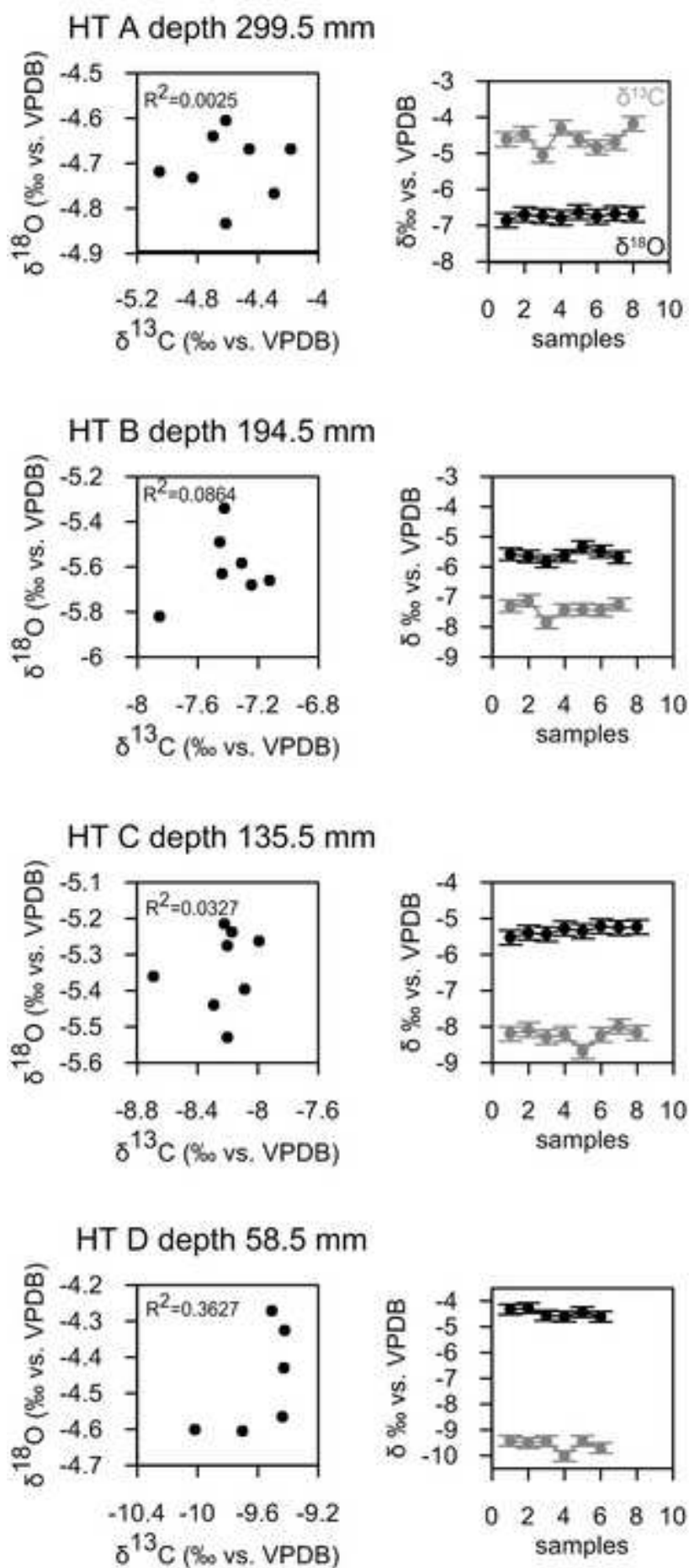


Figure 7
[Click here to download high resolution image](#)

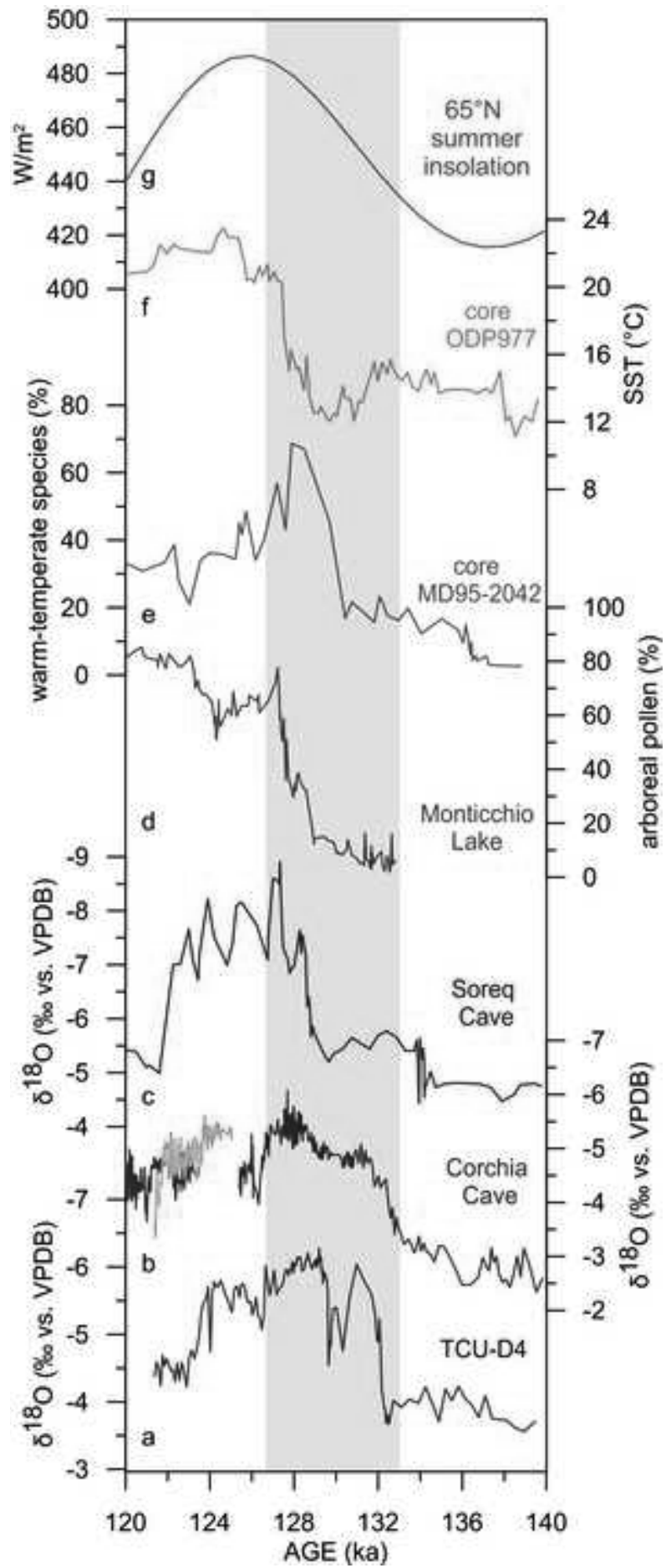


Figure 8
[Click here to download high resolution image](#)

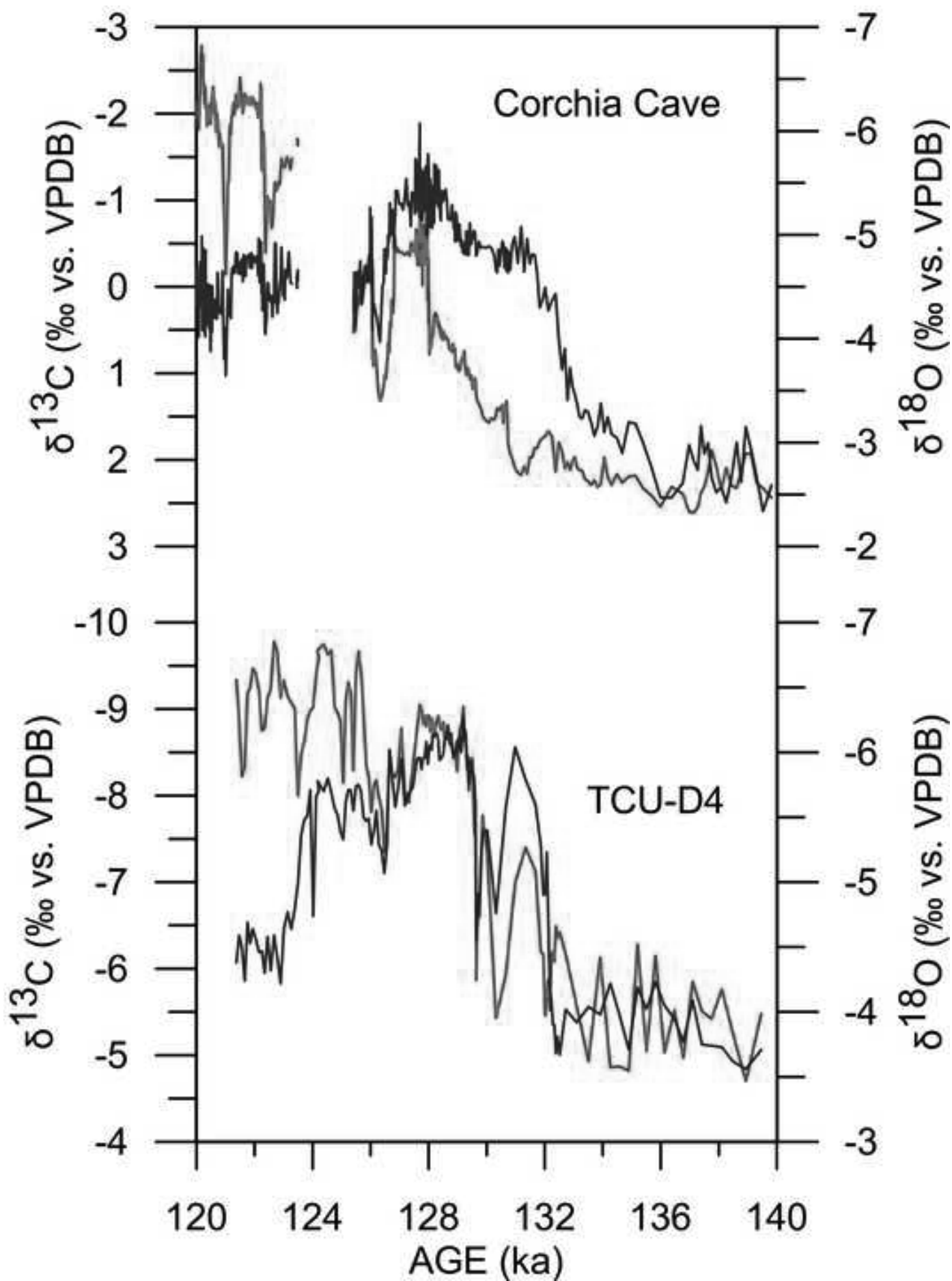


Figure 9
Click here to download high resolution image

